EasyChair Preprint

№ 8103

Detection of Internal Defects of CFRP Straighten Steel Structure Using Eddy Current Pulsed Thermography

Viplavi Dongare and Amey Khedikar

May 28, 2022

IC-DTSDG-22

Detection of internal defects in CFRP strengthened steel structures using Eddy Current Pulsed Thermography

Ms.Viplavi sanjay Dongare , *(Research Scholer)*
Department of Structural Engineering ,
Tulshiram Gayakwad Patil college of Engineering and Technology, Nagpur
viplavidongare90@gmail.com

Prof. Amey .R. Khedikar , *(Project Guide)*
Research scholer, Department of Structural Engineering ,
Tulshiram Gayakwad Patil college of Engineering and Technology, Nagpur
Amey.R.khedikar@gmail.com

Abstract-
This study investigates the effectiveness of eddy current pulsed thermography (ECPT) to detect internal defects in CFRP reinforced metal structures. Various internal common defects of CFRP reinforced steel structures are involved in this study, which include fragmentation, low impact impact on CFRP, metal cracking, and debonding on the CFRP / steel interface. Theoretically we have analyzed the impact of these problems on the magnetic and thermal reaction of structures. To confirm the results of the theater, statistical and diagnostic tests are performed on CFRP reinforced steel plates with various types of defects. Numerical and diagnostic results indicate that the observed malformations can be assessed by ECPT and shown as regions with low temperatures in ECPT thermograms. In addition to the thermal characteristics of thermograms, the emergence of the temperature profile and temperature changes are investigated in order to further analyze the thermal response in the CFRP environment. In addition, the effectiveness of ECPT in restoring the shape and size of errors is demonstrated based on the results of the tests. In general, theoretical, numerical and experimental results show that ECPT is effective in diagnosing internal defects in CFRP reinforced steel structures, indicating that ECPT provides a promising approach to such a complex complex structure.
Keywords--*Defects in Non-destructive testing, Thermal analysis CFRP strengthened steel structures, composite materials, structures, defects, damage, detection and evaluation, structural health monitoring etc.*

1. Introduction

Nowadays, carbon fiber reinforced plastic (CFRP) materials are widely used in many industrial applications, e.g. aerospace, automotive, public infrastructure, with excellent mechanical properties. Excellent and resistant to corrosion, heat and corrosion. Defects, such as input, delamination, foam, impact damage, destruction, can occur at the manufacturing stage or during use. Installation or embedding between layers of CFRP can weaken the complex machine structure, leading to a potential failure risk.
Carbon Fiber Reinforced Polymer (CFRP) is widely used in aircraft and wind turbine blades due to their high strength and low weight. CFRP is susceptible to impact damage and CFRP damage detection is essential for structural safety. This study was designed to detect the effects of attenuation using eddy current pulse temperature (ECPT) measurement.

CFRP: CFRP, short for Carbon Fiber Reinforced Plastic, is a composite consisting of carbon fiber and other materials or complements at a macroscopic level, capable of combining individual and optimal properties and hence the CFRP. shows better performance than its components. In an effort to develop new and improved aircraft equipment that must be strong, light and durable, researchers at the Royal Aircraft Facility, Farnborough, UK, produced carbon fiber in 1963-64. Used Totally, CFRP combines low weight with excellent mechanical properties and durability, and has been active in the aerospace, automotive

and shipbuilding industries for nearly four decades. Furthermore, in the past two decades, research institutes and industries have paid more attention and efforts to CFRP compounds as supporting components, especially in aerospace applications and car. On the other hand, there has been a huge increase in the availability of advanced substrate materials that serve as supporting components in CFRP, such as high-performance thermoplastics, and advances in the development of techniques. fast and reliable processing, greatly improving the development and use of CFRP.

2. Literature Survey

A. Taram et. al. 2016, In this eddy current temperature study, electromagnetic induction is used to induce heat flow in objects and record its temperature response using an infrared camera. Flaw detection is based on changes in heat distribution. It is an efficient and accurate means of detecting an implicit element in metallic objects and can be grown as pulse or amplitude modulated. This paper describes simulation operations using pulsed eddy current thermometers to detect defects and measure metal objects in transmission mode. Flux2D finite element software was used.

Xin Li et. Al. 2008, In this study, Limitation of non-corrosive methods in testing carbon fiber reinforced plastic (CFRP) compounds is a major issue in the practical application of the material, especially in the aviation industry. This paper presents a study aimed at the non-destructive expressions of CFRP using current vortex methods. The relationship between the signal of different types of induction probes and the microstructure of the CFRP samples was observed. Quantitative electrical activity measurement of an object based on the analytical solution of Deeds and Dodd, providing the basis for prediction and detection of defects in fibers and properties. Optical fiber orientation specifications have also been performed on omnidirectional and indirect CFRPs using highly focused investigations. Finally, a 3D finite element (FEM) computer simulation was performed to demonstrate the integration of the probes with the sample and support the experimental method. Chapter

Chuck Hellier and. al. 2009, In this paper, the fabrication of aluminum/carbon fiber reinforced plastic (CFRP) hybrid plate using eddy current sensor in many cases is presented in this paper. Circular air sensors and sensors with high ferritic core sensors are designed for bulk conductivity measurement and directional characterization. An analytical model describing the interaction of a circular sensor with a hybrid planar structure is developed. Finite element (FE) models that take into account the CFRP anisotropy are also proposed. Both models are in good agreement with the test results. The characteristics of sensory signals are analyzed and interpreted. This is believed to be the first published report on the use of current eddy current techniques in the production of aluminum/CFRP hybrid materials.

Literature Summary:

By studying various materials and methods, it has been confirmed that the Eddy Current Pulse Thermometer (ECPT) is one of the new diagnostic and test methods (NDT&E) has been used to check rail integrity, especially in communication fatigue (RCF) detection and crack sizing. This paper proposes a framework for exploratory analysis (POD) for ECPT system. In particular, three distinct features, namely high temperature response, first-order variance prediction, and first-order dissociated image map, are used to measure angular slit length by inserting a line. Based on the positive relationship between these factors and the clearance length, the POD curves of the ECPT system based on the coil line for angular strain detection were calculated and compared. The results show that the high temperature responsive element has high frequency and visibility obtained in a short space. Unique superlative image and rating board features are appealing to capture long spaces.

3. Project Methodology

On the basis of an interesting approach, efficient thermometers can also be divided into pulse electrochemicals (PT), heat-locking (beds), vibration (VT) and thermal thermoelectric (SHT). PT and illuminated are two main common processes. In both cases, the heat energy is transmitted to the object where the heat is distributed by diffusimer through the material. After that, a thermal reaction recorded by an infrared camera was observed to reveal the presence of characteristics. Tests can be done in two different ways. In transmission mode, infrared camera and sensor source are stored based on the surveyed sample. On the other hand, in display mode, infrared camera and joy source are placed in the same way in the sample during the investigation. In addition, a series of signal processing methods and filtration methods can be used to access incorrect information, including internal abnormalities and property characteristics.

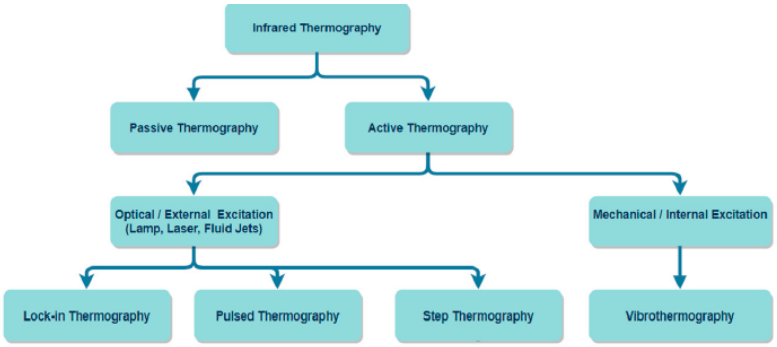

Figure 1. Classification of common infrared thermography techniques used in NDT.

4. Fundamental of ECPT

Based on the bases of ECPT, Figure 1 describes the common detection method of detecting defects in CFRP's reinforced steel structure. As shown in the picture. 1, Foucault lines are applied to metal parts and CFRP with current acute fluctuations in the frequency in the coil. As the spiritual streams were previously analyzed, the CFRP was very low and abandoned. Therefore, a small amount of thermal joule is manufactured in CFRP. At the same time, the corresponding temperature of joule's courage causes a significant increase in temperature in the metal section. The temperature slope between the metal and CFRP section causes a continuous increase in temperature and increases the temperature in CFRP. This thermal conduction ceases until a final thermal equilibrium is reached in the entire reinforced steel structure of the CFRP.

In the case of invalid detection, the presence of defects in the CFRP reinforced steel structure, including fragmentation between the CFRP layers, low velocity failure of CFRP, metal base cracking, and failure CFRP/steel interface, will affect the manufacturing process heat and heat transfer in a variety of ways. Such influences lead to an unusual temperature distribution in the CFRP region. This puzzling temperature distribution can be captured with a thermal imaging session. The presence of defects can be detected in the received heat graphs, and the defect properties can be restored by a specific temperature pattern recorded in the thermal graphs..

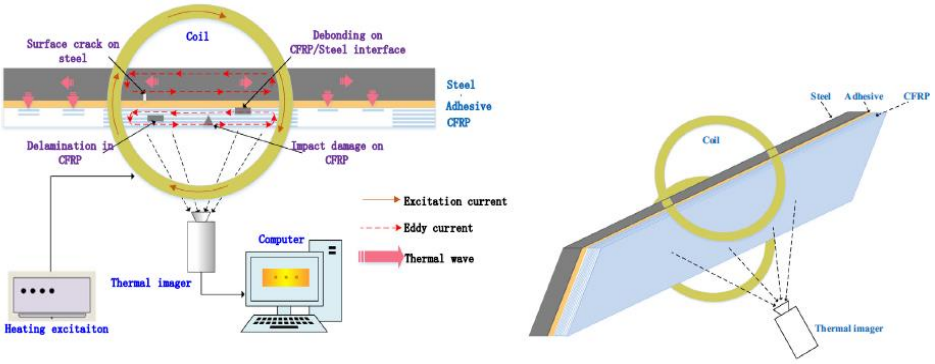

Fig. 2. Schematic of the proposed method for defects detection in CFRP.

5. Results and Discussions

The test was performed in a dark and closed room at Thermal Design and Infrared Laboratory of Kongju National University, Korea. The room temperature was set at 22 ^{o}C and the relative humidity was maintained at 48%. To test the front-end thermal response, the test sample was aligned, and the display mode was selected. The front of the sample is stimulated by pulse temperature for a period of approximately 10 ms. Thereafter, a thermal sample response was recorded for 5 seconds. Figure 5a shows a thermal image at 0 s recorded before the use of heat heart rate. Figure 5b shows a thermal image during the 0.1 second recorded after the input fluctuations in which the errors found show high signal brightness in the background without

performing any data processing techniques. Figure 5c shows the thermal image which is the result of removing Figure 5a from Figure 5b. The results showed that shallow errors have a large size clearly detected, and deep errors of small size were detected a little.

To investigate the geometric effects that do not work in the applied temperature change, the error response with a different aspect ratio (measure of width and depth) was analyzed. Errors A1, A4, C1, and C4 have an aspect ratio of 8.0, 6.0, 5.3, and 4.0, respectively, selected for investigation. The ROI of 4 _4 pixels in the center of each element was considered, and the average temperature was measured. Figure 6 shows the thermal response of selected errors about the 5 s period. It was found that the temperature obtained by the sample was faster than its decomposition due to the shorter pressure momentum. Over time, higher temperatures often reach equilibrium. It should be noted that the relatively thin A1 element with a high degree of visibility causes significant temperature difference compared to other problems with low aspect ratio. Variation in temperature distribution was sufficient to distinguish errors. However, thermal imaging processing is performed to reduce noise and improve visual acuity. The algorithms mentioned in Section 3 are compiled using MATLAB® R2019a.

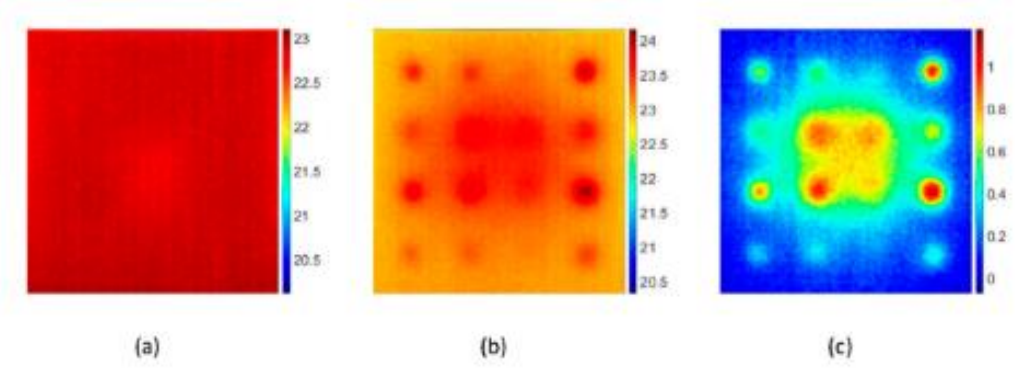

Figure 3. Thermal image of the anterior surface of the lower extremity specimen after pretreatment, (a) thermal image at 0 s before cardiac application, (b) thermal image at 0.1 s after temperature setting. the ability to change when the error indicates a high signal disparity from the background and (c) the thermal image obtained from the Figure 5a output in Figure 5b [Frequency = 50 Hz, number of frames = 250, output window end = 5 seconds]. Temperature in degrees Celsius.

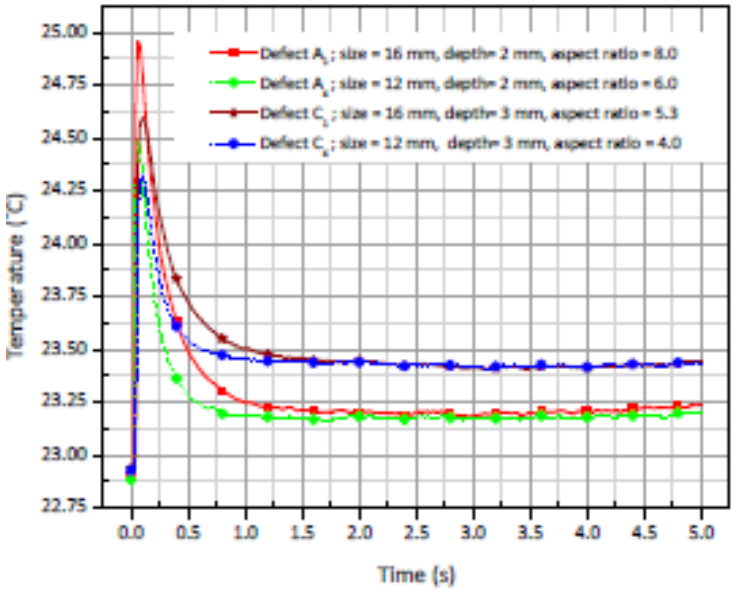

Figure 4. Detection of temperature profiles of flat holes in steel plate under heating temperature [Frequency = 50 Hz, number of frames = 250, termination window = 5 s].

5.1. Thermal Signal Reconstruction Results

TSR processing is applied to each pixel of the immature thermal image to reconstruct the logarithmic time dependence and outputs of the first and second coefficients. Logarithmic polynomial coefficients up to order of 8 were tested. To view the results of the TSR process, one thermal image for 0 s (Figure 5a) and one thermal image of 0.1 s (Figure 5b) were selected for further investigation. Figure 7 shows the TSR processing results of the selected thermal images. In Figure 7, the first column shows the TSR effects of the thermal image at 0 s; the second column shows the TSR effect of the thermal image at 0.1 s; the third column records the thermal image obtained after extracting the thermal image from the first column in the second column; column 4 shows the output of the first column of the thermal image and column 5 shows the output of the second column of the thermal image; different degrees of polynomial coefficients. It should be noted that the selection of the appropriate polynomial degree during the recovery process plays an important role in thermal data equivalence. To quantify the quality of the TSR insertion, the square root square error (RMSE) of each degree of polynomial insertion was evaluated. For this purpose, fault A1 class 8 was considered and the temperature measured at the installation level. Figure 8 shows the residuals and Table 1 presents the RMSE as a function of the numerical coefficients of the A1 element. Inverting the TSR by two coefficients was found to have a significant residual early in the cooling process. At three coefficients, residuals and RMSE begin to decrease and improve with this increase. In contrast, the results from the first and second extractions gave the best results with only three levels of polynomial activity, as shown in Figure 7b.

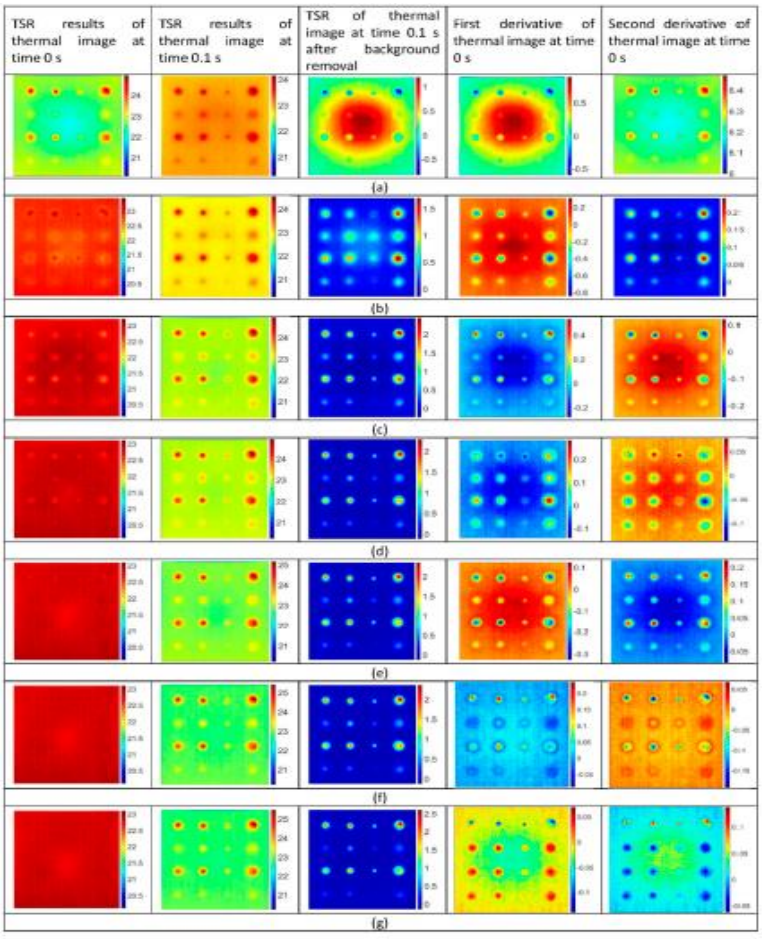

Figure 5. Comparison of pulsed thermography imaging images and reconstruction of thermal signal at times corresponding to polynomial insertion order, (a) order 2, (b) 3rd order, (c) 4th order, (d) 5th order, (e) 6th

order, (f) 7th order and (g) 8th [Frequency = 50 Hz, stand number = 250, termination window = 5 s]. Temperatures are in degrees Celsius.

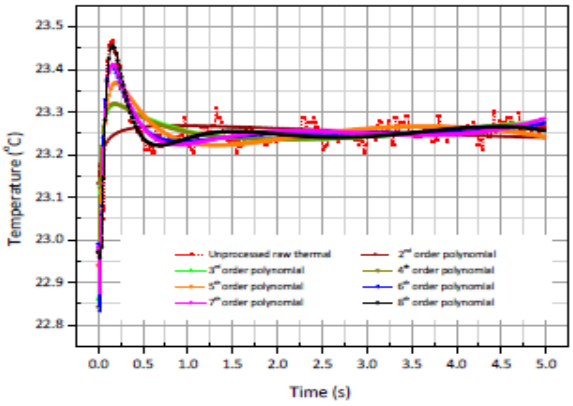

Figure 6. Time residues as a function of coefficient numerical values in the retraction of a 16 mm flat hole and a depth of 2 mm [Frequency = 50 Hz, number of frames = 250, cutting window = 5s].

Table 1. Root error refers to a square error as a function of the coefficient of numbers in the slope of a flat hole of 16 mm and a depth of 2 mm.

Degree of Polynomial Coefficient	Root Mean Square Error
2nd	0.0503
3rd	0.0396
4th	0.0395
5th	0.0326
6th	0.0263
7th	0.0255
8th	0.0200

5.2. Pulsed Phase Thermography Results

Figure 9 shows the effects of PPT in terms of frequency spectrum. It is noted that defect detection with PPT depends on the spectrum of the selected frequency. Figure 9a shows a phase image at 0.2 Hz, with no errors found. Figure 9b shows a phase image at 0.4 Hz, where errors are first detected but affected by sound. Figure 9c shows a phase image at 8 Hz, where a high degree of distortion is obtained with a high phase luminance.

Figure 9d shows a phase image at 25 Hz, where most of the feature information is lost. Figure 9e shows the phase image at 42.6 Hz, where the maximum number of defects is detected by the higher layer variation. It should be noted that the phase transition occurs at 42.6 Hz when the blue errors at 8 Hz have turned orange. Figure 9f shows an image of the 50 Hz frequency range, where the defect is again affected by sound.

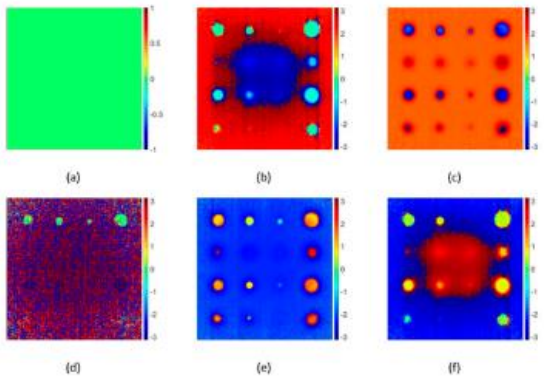

Figure 7. Stage image obtained by pulse-phase thermometry of a low-density steel plate after heating the heartbeat in different frequency spectrums, (a) 0.2 Hz, (b) 0, 4 Hz, (c) 8 Hz, (d) 25 Hz (e) 42.6 Hz and (f) 50 Hz, frame count = 250 frames, 5-second window pause. Ratio of phase angle in radians.

In order to select the most suitable frequency for the occurrence of strong attenuation and noise reduction, a covariance analysis of the A1 phase was carried out. For this, two RO _ 4 _ 4 pixels were considered, one in the center of the element and one in the nearest audio region. Figure 10 shows the phase difference of element A1 compared with the frequency spectrum. It is found that there are two positive frequencies for which the error shows a significant phase difference. The function shows a significant difference in the positive phase frequency of 8 Hz and a significant difference in the negative phase frequency at 42.6 Hz..

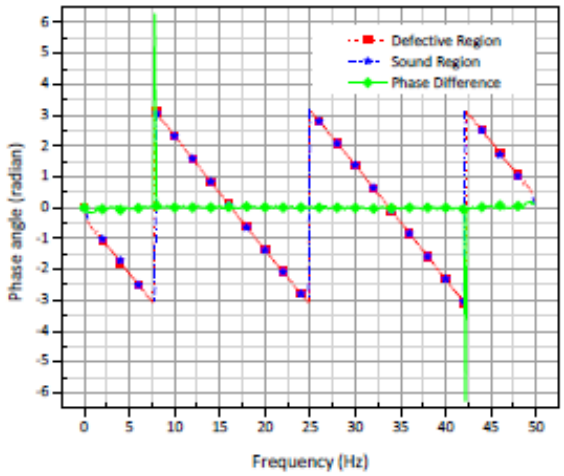

Figure 8. The profile of the distortion circuit regions with flat hole noise 16 mm and the steel plate depth of 2 mm detected by pulse phase thermometer method in terms of frequency; frequency band = 50 Hz, number of frames = 250 frames, duration 5 seconds.

5.3. Principle Component Thermography Results

Figure 11 shows the PCT results associated with EOFs. Unlike TSR and PPT, PCT results are less dependent on number of frames and frequency spectrum. The most important information is obtained from the first two EOFs.

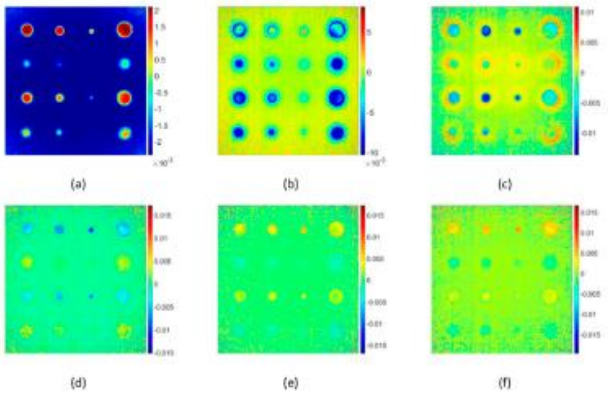

Figure 9. Pulsed thermography diagnostic images analyzed by systemic component EOF, (a) 1st EOF, (b) 2nd EOF, (c) 3rd EOF, (d) 4th EOF, (e) 5th EOF and (f) and 6th EOF. The ratings are in the "digital level" unit.

5.4. Comparison of Processing Techniques

The efficiancy of the three treatment strategies was measured in terms of improvement in disability detection and SNR. Three treatment strategies were scored based on improvement in disability detection and SNR. The best results given for each method are considered on a scale.

TSR results with 8th order polynomial adjustment, PPT effect over frequency.

5.4.1. Comparison Based on Defect Detectability

The defects found were 16mm and 12mm with aspect ratio greater than 3mm. TSR with 8th polynomial fit (Figure 7e) was able to detect 16 out of 16 defects. Even small defects wi
th a size of 4 mm and an aspect ratio of 0.8 are slightly detected. T at 0.8 Hz (Figure 9c) and T with the first EOF (Figure 11a) were able to detect 14 out of 16 anomalies.

5.4.2. Comparison Based on Signal to Noise Ratio

Two ROIs of 4 _ 4 pixels, one in the center of the element and the other in the nearest sound area,

$$\mathrm{SNR} = 20\log_{10}\left(\frac{|\mathrm{DROI}_{\mathrm{mean}} - \mathrm{SROI}_{\mathrm{mean}}|}{\sigma}\right)$$

where DROImean, SROImean, and represent, respectively, the arithmetic definition of ROI in a defective area.

location, arithmetic definition of ROI in the audio area, and general ROI deviation in the audio area.

The results obtained using equation (7) in the data are presented in Table 2. The results show that all three signal processing techniques significantly improve the SNR. PPT and PCT manage TSR according to SNR. It should be noted that PCT is dominant over PPT due to small deviation of 2 and 3 mm depth, while PPT is dominant due to small deviation of 4 mm and 5 mm depth. For example, in table 2 there is a shallow element A1; The green thermal image provides an SNR of 33.26 dB; The TSR provides an SNR of 40.46 dB, an increase of 21.64%; The PPT provides an SNR of 45.24 dB, an increase of 33.26%; PCT provides an SNR of 47.78 dB, an increase of 43.65%; compared to the picture. Likewise, due to B1 worm characteristics; The green thermal image provides an SNR of 19.18 dB; The TSR provides an SNR of 31.18 dB, an increase of 62.56%; The PPT provides an SNR of 46.28 dB, an increase of 141.29%; PCT provides an SNR of 41.6 dB, an increase of 116.89%; related to the hottest thermal image.

Table 2. SNR values for each processing techniques and flat-bottomed holes.

Defect ID.	SNR			
	Raw Image	TSR	PPT	PCA
A_1	33.26	40.46	45.24	47.78
A_2	-	32.39	42.15	44.56
A_3	-	39.18	43.92	47.15
A_4	28.17	39.47	44.56	47.72
B_1	19.18	31.18	46.28	41.60
B_2	-	26.15	-	-
B_3	-	31.75	33.65	31.90
B_4	12.19	28.78	40.76	38.85
C_1	32.14	38.98	46.55	46.58
C_2	-	32.29	36.52	34.91
C_3	-	39.47	45.41	45.58
C_4	28.39	38.28	45.90	46.76
D_1	23.96	28.78	47.12	44.52
D_2	-	15.62	-	-
D_3	-	27.82	45.91	40.26
D_4	21.44	27.64	47.10	44.16

Note: The symbol '-' is the representation of non-detected defects.

In this work, pulsed thermal measurement method is used in metal structure for the purpose of detecting wall defects. The basics of TSR, PPT, and PCT have been updated for thermal imaging and analysis. The efficiency of each signal processing was evaluated in terms of advanced feature rejection and SNR. Based on the results, it was determined that significant improvements in SNR feature detection capabilities and value could be achieved after strategy

implementation. The TSR provides lower resolution images than green thermal images and offers significant improvements in the selection of options through enhanced timing and position adjustments as well as the ability to ability to create images of time. However, variation of results in different cases or frameworks can be detrimental to TSR. PPT was found to be very sensitive to feature depth and provided the primary SNR for both small and deep flaws. However, the effects of PPTs are sometimes difficult to manage because they provide a lot of data for different spectra. PCT has been shown to be helpful in diagnosing problems large and small. Frame number independent results have proven to be a key advantage of PCT.

In addition, the ability to detect the maximum depth of pulsed thermodynamics will be investigated. In addition, TSR-based analysis will be performed. in the high polynomial insertion. Finally, error analysis strategies will also be considered for the results obtained.

6. Conclusion

In this study, the effectiveness of Eddy Current Pulse Temperature (ECPT) for detecting CFRP reinforced steel structures was analyzed and confirmed. Internal faults were investigated, including CFRP connection/metal interface, CFRP layer fragmentation, metal base cracking, and low-speed CFRP damage.

According to the results of theoretical analysis and testing, it is concluded that ECPT successfully detects various defects in reinforced steel structures before CFR, providing a promising and accurate method to ensure service life. of this composite structure. Future work will focus on ECPT's ability to detect other types of defects in CFRP/structural steel structures and the impact factors including adhesion, CFRP layer thickness and size of systematic tests.

In this work, pulsed thermography method is used in metal structure to detect wall defects.

The basics of TSR, PPT, and PCT have been updated for thermal imaging and analysis. The effectiveness of each signal processing method was evaluated based on improved defect detection and SNR. Based on the results, it was decided

That significant improvements in feature detection and SNR values could be achieved after strategy implementation. TSR provides lower resolution images than green thermal images and offers significant improvements in defect detection through enhanced spatial and temporal tuning as well as the ability to create time images. However, variation of results in different cases or frameworks can be detrimental to TSR.

PPTs were found to be very sensitive to feature depth and provide the primary SNR for both small and deep flaws. However, the effects of PPTs are sometimes difficult to manage because they provide a lot of data for different spectra. PCT has been shown to be helpful in diagnosing problems large and small. Frame T.

Future work will focus on using pulsed photothermal signal processing techniques to detect actual faults in pipeline structures. In addition, the Maximum depth detection capability of the pulse thermometer will be investigated. In addition, analysis based on TSR will be performed with high polynomial degree. Finally, error analysis strategies will also be considered for the results obtained.

References

[1] Emmanuel P. Papadakis, “Quality degradation due to shipment of nonconforming product under statistical process control in the absence of quarantining”, Materials Evaluation, Vol. 51(11), pp. 1274–1278, 1993.

[2] P J James, “The role of non-destructive testing in the control of boiler tube failures”, Insight, Vol. 37(2), pp. 179-183, 1995.

[3] Chuck Hellier, “Handbook of Non-destructive evaluation”, McGraw-Hill Professional, 2001, ISBN0-07-028121-1; ISBN0-07-139947-X.

[4] K. N. Hitchcock, “Design evaluation through improved non-destructive testing technology”, British Journal of NDT, Vol. 33(4), pp. 167-171, 1991.

[5] P.J. Heffernan, “Fatigue behaviour of reinforced concrete beams strengthened with CFRP laminates”, PhD thesis, Royal Military College of Canada, 1997.

[6] J. Waller, “Carbon fibre cement composites”, Civil Engineering and Public Works Review 67, 789, pp. 357—361, 1972.

[7] M. P. De Goeje and K. E. D. Wapenaar, “Non-destructive inspection of carbon fibre-reinforced plastics using eddy current methods”, Composites, Vol. 23(3), pp. 147-157, 1992.

[8] Barret R, “All-moving active aerodynamic surface”, Research in Smart Materials and Structures, Vol. 4, pp. 65-71, 1995.

[9] Hanselka H, “Realization of smart structures by using fiber composite materials”, Smart Mechanical Systems-Adaptronics, pp. 1-10, Dusseldorf, 1997.

[10] A. Briggs, “Review: Carbon fibre-reinforced cement”, Journal of Materials Science, Vol. 12, pp. 384—404, 1977.

[11] McGuire, M.F. Stainless Steels for Design Engineers; ASM International: Materials Park, OH, USA, 2008.

[12] Baddoo, N. Stainless Steel in Construction: AReview of Research, Applications, Challenges and Opportunities. J. Constr. Steel Res. **2008**, 64, 1199–1206. [CrossRef]

[13] Lister, D.H.; Cook, W.G. Nuclear Plant Materials and Corrosion

Available online:https://www.unene.ca/essentialcandu/pdf/14%20-%20Nuclear%20Plant%20Materials%20and%20Corrosion.pdf (accessed on 2 June 2020).

[14] Okada, H.; Uchida, S.; Naitoh, M.; Xiong, J.; Koshizuka, S. Evaluation Methods for Corrosion Damage of Components in Cooling Systems of Nuclear Power Plants by Coupling Analysis of Corrosion and Flow Dynamics (V) Flow-Accelerated Corrosion Under Single-and Two-Phase Flow Conditions. J. Nucl. Sci. Technol. **2011**, 48, 65–75. [CrossRef]

[15] Ahmed, W.H. Flow accelerated corrosion in nuclear power plants. In Nuclear Power-Practical Aspects; Anonymous, Ed.; IntechOpen: Rijeka, Croatia, 2012.

[16] Naitoh, M.; Okada, H.; Uchida, S.; Yugo, H.; Koshizuka, S. Evaluation Method for Pipe Wall Thinning due to
Liquid Droplet Impingement. Nucl. Eng. Des. **2013**, 264, 195–202. [CrossRef]

[17] Onel, Y.; Ewert, U.; Willems, P. Radiographic Wall Thickness Measurement of Pipes by a New Tomographic Algorithm. In Proceedings of the 15th WCNDT, Roma, Italy, 15–21 October 2000; pp. 1–6.

[18] Edalati, K.; Rastkhah, N.; Kermani, A.; Seiedi, M.; Movafeghi, A. The use of Radiography for Thickness Measurement and Corrosion Monitoring in Pipes. Int. J. Press. Vessel. Pip. **2006**, 83, 736–741. [CrossRef]

[19] Rakvin, M.; Markuˇciˇc, D.; Hižman, B. Evaluation of PipeWall Thickness Based on Contrast Measurement using Computed Radiography (CR). Procedia Eng. **2014**, 69, 1216–1224. [CrossRef]

[20] Ju, Y. Remote measurement of pipe wall thinning by microwaves. In Advanced Nondestructive Evaluation II: Volume 2; Anonymous, Ed.;World Scientific: Busan, Korea, 2008; pp. 1128–1133.

[21] Liu, L.; Ju, Y. A High-E_ciency Nondestructive Method for Remote Detection and Quantitative Evaluation of Pipe Wall Thinning using Microwaves. NDT E Int. **2011**, 44, 106–110. [CrossRef]

[22] Liu, L.; Ju, Y.; Chen, M. Optimizing the Frequency Range of Microwaves for High-Resolution Evaluation of Wall Thinning Locations in a Long-Distance Metal Pipe. NDT E Int. **2013**, 57, 52–57. [CrossRef]

[23] Nishino, H.; Takemoto, M.; Chubachi, N. Estimating the Diameter Thickness of a Pipe using the Primary Wave Velocity of a Hollow Cylindrical GuidedWave. Appl. Phys. Lett. **2004**, 85, 1077–1079. [CrossRef]

[24] Leonard, K.R.; Hinders, M.K. Lamb Wave Tomography of Pipe-Like Structures. Ultrasonics **2005**, 43, 574–583. [CrossRef]

[25] Cheong, Y.; Kim, K.; Kim, D. High-Temperature Ultrasonic Thickness Monitoring for Pipe Thinning in a Flow-Accelerated Corrosion Proof Test Facility. Nucl. Eng. Technol. **2017**, 49, 1463–1471. [CrossRef]

[26] Alobaidi, W.M.; Kintner, C.E.; Alkuam, E.A.; Sasaki, K.; Yusa, N.; Hashizume, H.; Sandgren, E. Experimental Evaluation of Novel Hybrid Microwave/Ultrasonic Technique to Locate and Characterize PipeWall Thinning. J. Press. Vessel Technol. **2018**, 140, 011501. [CrossRef] 17. Jinfeng, D.; Yihua, K.; Xinjun, W. Tubing Thread Inspection by Magnetic Flux Leakage. NDT E Int. **2006**, 39, 53–56. [CrossRef]

[27] Zhang, Y.; Yan, G. Detection of Gas Pipe Wall Thickness Based on Electromagnetic Flux Leakage. Russ. J. Nondestruct. Test. **2007**, 43, 123–132. [CrossRef]